

Geothermal potential assessment of the Nevado del Ruiz volcano based on rock thermal conductivity measurements and numerical modeling of heat transfer

Maria Isabel Vélez^a, Daniela Blessent^b, Sebastián Córdoba^b, Jacqueline López-Sánchez^b, Jasmin Raymond^a, Eduardo Parra-Palacio^b

^aInstitut national de la recherche scientifique, Centre Eau Terre Environnement, Québec, Qc, Canada

^bUniversidad de Medellín, Programa de Ingeniería Ambiental, Medellín, Colombia.

Abstract

This work presents an estimation of the geothermal potential of the Nevado del Ruiz (NDR) volcano, bridging the knowledge gap to develop geothermal energy in Colombia and improve resource estimates in South America. Field work, laboratory measurements, geological interpretations, 2D numerical modeling, and uncertainty analysis were conducted to the northwest of the NDR to assess temperature at depth and define thermal energy content. About 60 rock samples were collected at outcrops to measure thermal conductivity with a needle probe. A 2D numerical model, built from an inferred geological cross-section, was developed with the software OpenGeoSys to simulate the underground temperature distribution and then estimate the geothermal potential of a 1 km² area with sufficient temperature, assuming a recovery factor equal to 2.4% and a 30 years exploitation time. Coupled groundwater flow and heat transfer were simulated in steady-state considering two different thermal conductivity scenarios. Results show that the average estimated potential is $1.5 \times 10^{-2} \text{ MW}_t \text{ m}^{-1}$ of the reservoir thickness, considering temperatures greater than 150 °C located at a depth of approximately 2 km, in a selected area situated outside of the Los Nevados National Natural Park (NNP), to avoid any direct intervention on this protected area. According to a Monte Carlo analysis considering pessimist and optimist scenarios of thermal conductivity, the estimated geothermal power was $1.54 \times 10^{-2} \text{ MW/m}$ ($\sigma = 2.91 \times 10^{-3} \text{ MW/m}$) and $1.88 \times 10^{-2} \text{ MW/m}$ ($\sigma = 2.91 \times 10^{-3} \text{ MW/m}$) for the two modeling scenario considered.

Keywords:

Nevado del Ruiz, Colombia, geothermal potential, thermal conductivity, OpenGeoSys

1 **1. Introduction**

2 Estimation of the worldwide geothermal potential is a challenging task, with pitfalls due to
3 uncertainties and knowledge gaps (Bertani, 2009). This worldwide potential is usually determined
4 by adding up the estimates for individual countries or regions, but the task is difficult, since the
5 geothermal energy potential is unknown in many countries (Stefánsson, 1998; Fridleifsson, 2003;
6 Stefánsson, 2005). This lack of information is particularly important for developing countries of
7 Latin America such as Colombia, where field data are sparse, if not non-existent. In the recent
8 report published by Bertani (2016), Colombia is indicated as a country where there is no geothermal
9 development yet and no additional information is provided. This situation is not unique to Colombia
10 but common to South America where untapped geothermal resources still need to be defined.
11 Recent studies on the estimation of the geothermal potential have been conducted in few countries
12 of South America, where there are no operating geothermal power plants. Aravena et al. (2016)
13 estimated the geothermal potential of high enthalpy geothermal areas of Chile to 659 MWe,
14 applying numerical methods and including inferred resources. Invernizzi et al. (2014) described a
15 preliminary assessment of the geothermal potential of Rosario de la Frontera area to the northwest
16 of Argentina, indicating 5.6×10^{18} J of heat stored in the rock and 0.8×10^{18} J in the geothermal fluids.
17 Ongoing exploration has taken place in Bolivia at the Laguna Colorado Field, while an estimation
18 of 150 MWe has been indicated for two geothermal fields in Peru (Bertani, 2016).
19 Such geothermal resource assessment depends on a variety of aspects that can be grouped as
20 follows: geological, physical, technological, and economical (Muffler and Cataldi, 1978). The
21 choice of a method for reservoir assessment depends on the available data, the purposes of the
22 assessment and the accuracy needed (Barylo, 2000). Muffler and Cataldi (1978) grouped the
23 methods for geothermal resource assessment in four categories: 1) surface heat flux method, 2)
24 volume method, 3) planar fracture method, and 4) magmatic budget method. The volumetric
25 method is commonly used for geothermal potential estimation at the early stage of geothermal
26 resource assessment. This method can be used when there are no or not enough exploratory wells

27 nor permeability data and is thus a preferred option for early stage assessment. A recovery factor is
28 considered by the volumetric method to calculate the static heat reserve in the reservoir and
29 estimates the extractable energy (Barylo, 2000). Stochastic simulations and risk analysis are
30 frequently used in conjunction with the volume method to estimate the range and the probable
31 distribution of stored heat reserves and exploitable energy. These analyses have been borrowed
32 from the oil industry, where they have been used for a long time to estimate probabilistic
33 hydrocarbon-in-place and oil and gas reserves in sedimentary basins (Ofwona, 2008). Such
34 stochastic simulations, commonly based on the Monte Carlo method, are particularly beneficial
35 where data is scanty and uncertainties high (Ofwona, 2008).

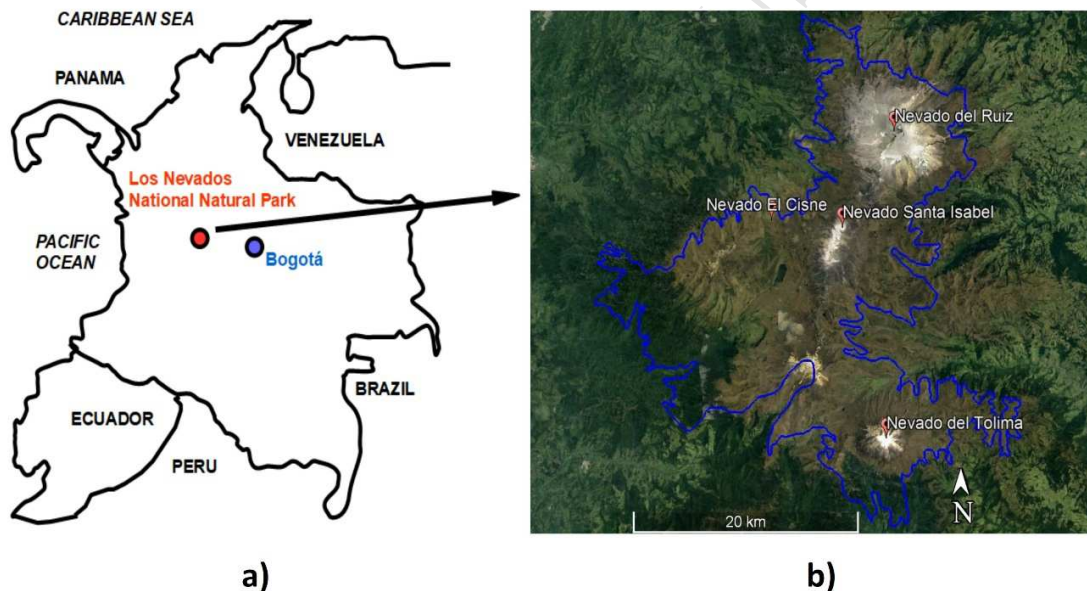
36 This work is an attempt to bridge the knowledge gap in Colombia and South America by describing
37 the geothermal potential assessment of an area of the Nevado del Ruiz (NDR) volcano located in
38 the Colombian Central Cordillera. Similar geological settings can be expected for geothermal fields
39 of the Colombian Central Cordillera, where the described method could be applied. The geothermal
40 resource assessment of the NDR volcano was actually based on 1) thermal conductivity laboratory
41 measurements on rock samples collected at outcrops, 2) an inferred geological cross-section, 3)
42 coupled groundwater flow and heat transfer numerical modeling with the OpenGeoSys software
43 (Böttcher et al., 2016), 4) volumetric resource estimation method, and 5) uncertainty analysis
44 conducted with the @RISK software (Ofwona, 2008; Walsh, 2013; Yang et al., 2015). The NDR
45 volcano is the best known geothermal area of Colombia, where the interest of several entities
46 converge (Alfaro, 2015). However, geothermal development in Colombia is incipient in comparison
47 with other Latin America countries with similar volcanic environments (Bertani, 2016). This case
48 study of the NDR area contributes to fill this lack of information and to help develop the geothermal
49 potential in Colombia.

50

51

52 2. Geological settings

53 Volcanism in the Colombian Central Cordillera is defined by a complex tectonic framework, since
 54 the country is located at the intersection of South America, Nazca, and Caribbean tectonic plates.
 55 The subduction of the Nazca below the South American Plate is the governing mechanism
 56 triggering volcanic activity due to the rapid convergence of 58 mm/year occurring at the Colombia-
 57 Ecuador trench (Trenkamp et al., 2002). The NDR is an active stratovolcano enclosing the Los
 58 Nevados National Natural Park (NNP) covering an area of approximately 58300 hectares in the
 59 middle of the Colombian Central Cordillera ($4^{\circ} 53'43''$ N, $75^{\circ} 19'21''$ W), between the limits of
 60 Caldas and Tolima departments of Colombia (Figure 1).



61 **a)**
 62 Figure 1. a) Location of the Los Nevados NNP in Colombia and b) its neighboring Colombian
 63 departments (Risaralda, Caldas, Tolima, Quindío) and the main volcanoes (modified from Parques
 64 Nacionales Naturales de Colombia, 2007)

65 The NDR is part of the volcanic complex Ruiz-Tolima and contains three craters: the Olleta, the
 66 Piraña, and the Arenas. The Arenas crater has been the source of the most recent activity: an
 67 explosive eruption occurred in November 1985 (Naranjo et al., 1986), while variations in the

68 volcanic activity and ash emissions have been registered since October 2010 until these days¹.
69 Based on seismicity, geochemistry and geology of the volcano, Londoño and Sudo (2002) presented
70 a conceptual model of its activity, identifying three heat sources located at different depths: the first
71 one from 2 to 3 km, the second one from 5 to 10 km, and the deepest zone from 10 to 15 km. Stix et
72 al. (2003) presented a conceptual view of magma ascent through a plexus of cracks in the crust,
73 from the source main reservoir located at depth comprised between 9 and 15 km.

74 The geological situation of the Ruiz region is featured by several Tertiary and Quaternary volcanic
75 edifices and by a number of thermal springs. The reconstruction of the stratigraphic sequences is
76 difficult because the oldest metamorphic and sedimentary rocks located at the base of the volcanic
77 complex are often crossed or covered by igneous rocks that obliterate contacts (Arango et al., 1970).
78 Among all geological units described by González (2001), those that are identified in the inferred
79 geological cross-section described later, are the Cajamarca metamorphic complex (Pes), the
80 Quebradagrande Complex (Kvc and Ksc), the Andesite unit (NgQa), pyroclastic rocks (Qto), glacial
81 deposits (Qg), volcanic mud flows or lahars (Qfl), and recent alluvial deposits (Qar). The
82 Cajamarca metamorphic complex, which makes up the regional basement of the Colombian Andes,
83 encloses a wide range of lithological types. The pelitic complex (Pes) includes phyllites, sericite,
84 and mica schists. There is evidence that this complex has undergone a greenschists facies
85 metamorphism, while, locally, some rocks belonging to the amphibolites facies can be observed.
86 The Quebradagrande Complex is composed of sedimentary rocks (Ksc), such as black shales,
87 sandstones, conglomerates, limestones, with dynamic metamorphism and occasionally fossils.
88 Volcanic rocks (Kvc), such as basalts, pyroclastic flows and diabasic dykes, have undergone
89 prehnite-pumpellyite facies metamorphism. The Andesite unit (NgQa) has a composition ranging
90 from andesitic to dacitic, and basaltic at fewer locations. The andesitic flows are macroscopically
91 homogenous and have a porphyritic texture. The lahars or volcanic mud flows (Qfl) include blocks
92 of andesitic-dacitic lava with variable diameter from few centimeters to more than 5 m. The

¹ <http://www2.sgc.gov.co/Manizales.aspx>

93 pyroclastic rocks (Qto) may reach a thickness of 30 m. The recent alluvial deposits (Qar) cover
94 older rocks close to rivers and creeks and have a variable thickness, which is generally less than
95 20 m. The glacial deposits (Qg) are associated to the Pleistocene glaciations that covered the
96 Colombian Central Cordillera above 3000 m a.s.l.

97

98 **3. Previous studies on the Nevado del Ruiz geothermal resources**

99 The first geothermal study on the Nevado del Ruiz site was conducted towards the end of the 1960s
100 by the Italian company ENEL (Ente Nazionale per la Energia Elettrica) in collaboration with the
101 CHEC (Central Hidroeléctrica de Caldas) and described litho-stratigraphic features, volcanology,
102 structural events and hydrogeology of the NDR complex (Arango et al., 1970). Based on isotopic
103 analysis, Arango et al. (1970) proposed a first tentative hypothesis of a shallow hydrothermal
104 system clearly separated from a deep regional system. They identified the presence of a thick
105 caprock, formed by the upper part of the metamorphic complex and separating the two major
106 circulation-systems to the west, northwest and north of the Ruiz edifice. CHEC subsequently
107 published a technical report describing the geological context of the NDR with details about the
108 volcanology, geochemistry and geophysical characteristics of the area (CHEC et al., 1983). Two
109 years after, the NDR volcano erupted during November 1985 (Melson et al., 1990; Thouret, 1990;
110 Vatin-Pérignon et al., 1990), causing the Armero tragedy with about 25 000 casualties and leaving
111 aside the geothermal explorations.

112 Field work restarted only in 1997 when the only deep geothermal exploration well in Colombia
113 (Las Nereidas well) was drilled to a depth of 1466 m on the western side of the NDR, at 3450 m
114 a.s.l.. In this borehole, seven lithological units with hydrothermal alteration were identified. The
115 measured bottom hole temperature was about 200 °C (Monsalve et al., 1998). Recent studies were
116 conducted from 2011 to 2013: Rayo-Rocha and Zuluaga (2011) indicated, through petrographic and
117 geochemical analysis of lava samples, the existence of a deep magmatic chamber feeding a
118 shallower chamber. Rojas (2012) presented the temperature profiles measured in three 300 m deep

119 wells that were drilled in 2011 with the objective to measure the geothermal gradient. Forero (2012)
120 provided a characterization of hydrothermal alteration to the northwest of the volcano that led to a
121 simple conceptual model of the geothermal reservoir. Almaguer (2013) presented the results from a
122 magnetotelluric study conducted to the North of the volcano, where high electrical conductivity
123 areas confined by sections of moderated resistivity were interpreted as a possible reservoir and
124 caprock, respectively. After this renewed interest, the Colombian ISAGEN company then applied
125 for an environmental license following the realization of the environmental impact study to drill the
126 first of five planned exploratory wells on the western flank of the NDR volcano (Alfaro, 2015).
127 González-García and Jessell (2016) published a first 3D geological model for the Ruiz-Tolima
128 volcanic massif, using the Monte Carlo method to characterize geological uncertainty. Their model
129 represents the probability of occurrence of geological units, suggesting where future exploratory
130 work should be conducted.

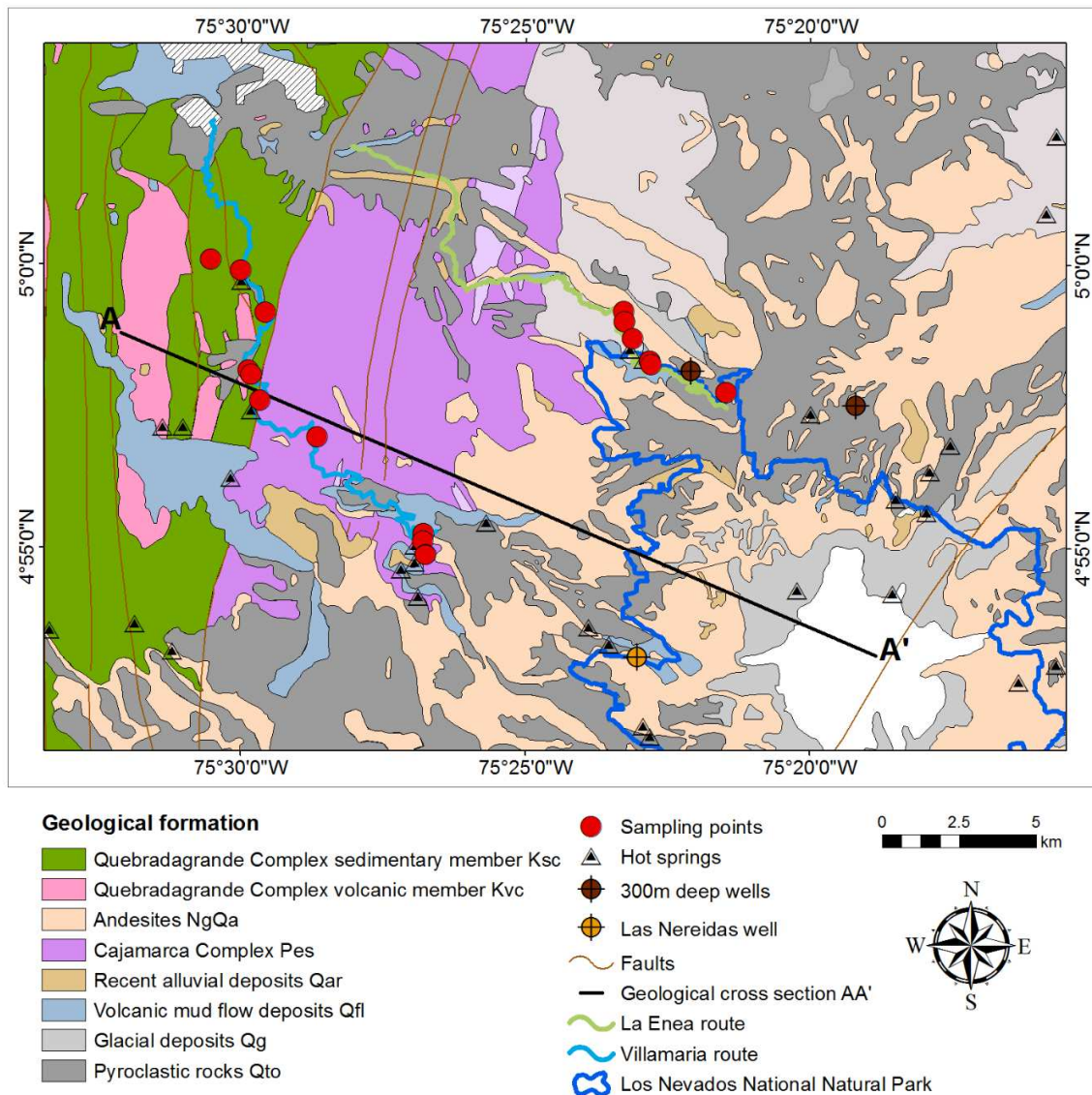
131

132 **4. Material and methods**

133 **4.1 Rock sampling and geological cross-section**

134 Field work was conducted in November 2014 over two itineraries with an approximate length of
135 26 km (Villamaria and Enea route) outside of the Los Nevados NNP (Figure 2). The objective of
136 rock sampling was to collect the main lithologies characterizing the study area. Three rock samples
137 were collected at each sampling locations (Table 1). The geological cross-section AA' (Figure 2)
138 starts from the NDR peak (A') and goes up to the outcrops of the Quebradagrande Complex (Ksc
139 and Kvc), located on the northwest of the NDR peak. The cross-section is drawn close to the
140 sampling points and hot springs located along the Villamaria route and crosses the Cajamarca
141 Complex (Pes), which is one of the lithologies of most interest, because this metamorphic complex
142 might be part of a potential geothermal reservoir (Almaguer, 2013), together with the
143 Quebradagrande Complex (CHEC, 1983). Although this hydrothermal system has been studied
144 since the seventies, the location of a porous reservoir is not publicly known, but it is suggested that

145 faults provide structural control of the hydrothermal flow (González-García et al., 2015).
 146 Geological observations indicate that the primary porosity of potential reservoir units is low and the
 147 potential to find natural hydrothermal systems is related to secondary porosity. However, faults
 148 were not considered in this work since the objective is to provide a quantitative methodology to
 149 estimate the geothermal resource potential based on heat stored in the basement rock. Fault zones
 150 shall be considered in further studies as structural geology information becomes available together
 151 with 3D geological models to provide a more accurate estimation of this geothermal potential.
 152



153
 154

Figure 2. Geological map of the study area showing the sampled outcrops. Simplified from

155 INGEOMINAS geological maps sheet Nos. 206 and 225 (Mosquera et al., 1998a; Mosquera et al.,
156 1998b).

157 4.2 Thermal conductivity measurements

158 Thermal conductivity measurements were made at the Institut national de la recherche scientifique
159 Centre Eau Terre Environnement (INRS-ETE) in Québec City (Canada), following the ASTM
160 methodology (ASTM, 2008). Thermal conductivity was measured inserting the KD2 Pro transient
161 needle probe RK- 1 (Decagon Devices Inc., 2008) in a 3.9 mm diameter hole previously drilled in
162 each rock sample that has been previously saturated when having visible porosity. The hole,
163 approximately 6 cm deep, was drilled with a rotary hammer in the middle of a flat side of each rock
164 sample, to ensure uniform heat transfer in every direction in the sample during the measurement.
165 The space between the needle and the hole was filled with thermal grease to ensure thermal contact.
166 The heating needle had a temperature sensor. Heat was injected through the needle for 5 minutes,
167 while temperature was monitored, and a 5 minutes recovery period was considered after the heating
168 pulse. The thermal conductivity was determined from the analysis of the temperature increment ΔT ,
169 which depends on the distance r from the source and on the time t , according to the infinite line
170 source equation (Carslaw and Jaeger, 1947):

$$171 \quad \Delta T(r, t) = \frac{-q}{4\pi\lambda} E_i \left(\frac{-r^2}{4\alpha t} \right) \quad (1)$$

172 where q (W m^{-1}) is the heat input per unit length, α ($\text{m}^2 \text{s}^{-1}$) is the thermal diffusivity, r (m) is the
173 needle radius, E_i is the exponential integral that can be developed as a Taylor series, λ ($\text{W m}^{-1} \text{K}^{-1}$) is
174 the thermal conductivity of the rock sample, and t (s) is the time. From Eq. 1, the temperature can
175 be approximated to a linear equation in a semi-logarithmic plot, where the slope is related to the
176 thermal conductivity λ :

$$177 \quad T(t) \approx \frac{q}{4\pi\lambda} \ln(t) + C \quad (2)$$

178 Thermal conductivity measurements were performed automatically at time intervals of 1 hour to
179 ensure that temperature returned to the equilibrium before doing a new measurement. Before and
180 after each measurement, calibration was required to determine the correction factor CF (Eq. 3),
181 which compares the thermal conductivity of a known material ($\lambda_{material}$), a standard plastic cylinder
182 supplied with the KD2 Pro thermal properties analyzer, with the one obtained experimentally
183 ($\lambda_{measured}$), to adjust the measured thermal conductivity (ASTM, 2008):

$$184 \quad CF = \frac{\lambda_{material}}{\lambda_{measured}} \quad (3)$$

185 **4.3 Heat capacity estimation**

186 Heat capacity was estimated according to the mesoscopic characterization of each rock sample
187 based on the values provided by Waples and Waples (2004). Although approximate, this estimation
188 is suitable since heat capacity does not show large variation within different rock types. The great
189 majority of the specific heat capacities of minerals at ± 20 °C is between 600 to 900 ($J\ kg^{-1}\ K^{-1}$), with
190 a strong preference for values between 800 and 900 ($J\ kg^{-1}\ K^{-1}$).

191

192 **4.4 Numerical modeling**

193 To provide an estimation of the geothermal potential for the study area, numerical modeling was
194 performed, since analytical methods can difficultly cope with irregular topography. It has long been
195 recognized that topography affects heat flow and topographic correction has been based on
196 identification of valleys and hills (Westaway and Younger, 2013). Nevertheless, the topography of
197 the geological cross-section AA' has a saw-tooth like profile (Figure 3) rather than a valley or a hill.
198 Therefore, numerical modeling allowed considering almost the real topography in the simulated
199 domain. The software OpenGeoSys (OGS), a scientific open-source initiative for numerical
200 simulation of thermo-hydro-mechanical/chemical processes in porous and fractured media
201 (Böttcher et al., 2016), was used to build a numerical model to estimate underground temperature
202 and quantify geothermal resources. The GMSH mesh generator (Geuzaine and Remacle, 2009) and

203 the Tecplot software were used to build the mesh and to visualize the numerical results,
 204 respectively. Fully saturated steady-state groundwater flow and heat transfer were the physical
 205 processes considered. Governing equations and specifications for modeling of geothermal processes
 206 were presented in detail by Böttcher et al. (2016) and therefore are not repeated here.

207

208 **4.5 Geothermal resources evaluation**

209 The quantification of geothermal resources was achieved for an area characterized by a temperature
 210 greater than 150 °C located outside of the Los Nevados NNP, at a depth between 2 and 3 km, and at
 211 a distance of 14 to 15 km from the left-hand side of the geological cross-section AA' (Figure 3). An
 212 area of 1 km² was considered for the estimation of the geothermal potential, since the reservoir
 213 spatial delimitation is currently uncertain and needs further field investigations, such as geophysical
 214 surveys, to better identify permeable formations. Both temperature (150 °C) and depth (3 km) are
 215 the recommended values based on economic feasibility of geothermal exploration in Colombia
 216 (Bernal et al., 2000). The temperature of 150 °C can also be used to define high enthalpy systems
 217 according to Lee (1996).

218 Subsurface heat stored was evaluated in the zone of interest (Figure 3) with the following equation:

$$219 \quad Q_r = \rho \cdot C \cdot A \cdot (T_d - T_0) \quad (4)$$

220 where Q_r (J m⁻¹) is the available subsurface heat per unit width of the reservoir, ρ (Kg m⁻³) is the
 221 rock density, C (J Kg⁻¹ K⁻¹) is the rock heat capacity, A (m²) is the area surrounding each selected
 222 point in the zone of interest, T_d (K) is the temperature at depth in the zone of interest and T_0 (K) is
 223 the temperature at the surface. Eq. (5) gives the total accumulated heat stored in the subsurface, but
 224 only a part of this quantity can be actually extracted. Therefore, the geothermal potential was
 225 estimated considering a recovery factor R , which is related to the available and exploitable energy
 226 (Calcagno et al., 2014) and depends on the porosity and on the permeability of the lithological
 227 formations of the geothermal reservoir (Walsh, 2013). The geothermal potential P_G (W) was finally
 228 calculated considering resource exploitation for a time t equals to 30 years:

$$P_G = R \cdot \frac{Q_r}{t} \quad (5)$$

229 In this case study, the geothermal potential was calculated using a recovery factor $R = 2.4\%$, which
 230 was reported by Calcagno et al. (2014) as the minimum recovery factor for fractured aquifers, as the
 231 potential NDR reservoir is hosted in low permeability basement rocks crossed by regional faults.
 232 Faults are expected to have an impact on the circulation of hydrothermal fluids in the NDR
 233 geothermal reservoir (Mejía et al., 2012). Further studies will consider the effect of faults, which do
 234 not cross the zone of interest selected in this work based on outcrops visited during field work.
 235 Conductive and advective heat transfer through the low-permeability rock matrix are the main
 236 processes considered in this study to provide a first estimate of the heat content in order to calculate
 237 geothermal resources.

238 Uncertainty analysis was conducted with Monte Carlo simulations using the @RISK software. The
 239 variables considered for uncertainty analysis were the temperature at depth T_d and the recovery
 240 factor R . T_d depends on the thermal conductivity and on the heat flow according to steady-state heat
 241 transfer that is conduction dominated in the numerical model.

242

243 5 Results

244 5.1 Laboratory measurements

245 The lithologic units identified at the 18 sampling locations (Table 1) were the Quebradagrande
 246 sedimentary Complex (Ksc), the Cajamarca Complex (Pes), the Andesite unit (NgQa) and the
 247 volcanic mud flow or lahars (Qfl). The Quebradagrande volcanic complex (Kvc) was not collected
 248 in the field since the access route did not lead to its outcrop (Figure 2).

249 Table 1: Sampling points coordinates and mesoscopic characterization

Sample #	Code	X coordinate*	Y coordinate*	Lithologic unit	Rock type
1	2014 MI 1	4.998	-75.500	Quebradagrande Complex	Sandstone
2	2014 MI 2	5.002	-75.509	Quebradagrande Complex	Sandstone
3	2014 MI 3	4.986	-75.493	Quebradagrande Complex	Sandstone

4	2014 MI 4	4.969	-75.498	Quebradagrande Complex	Schist
5	2014 MI 5	4.968	-75.497	Quebradagrande Complex	Schist
6	2014 MI 6	4.968	-75.497	Cajamarca Complex	Quartz phyllite
7	2014 MI 7	4.960	-75.495	Cajamarca Complex	Schist
8	2014 MI 8	4.986	-75.388	Andesite unit	Andesitic lava flows
9	2014 MI 12	4.972	-75.380	Andesite unit	Andesite
10	2014 MI 13	4.972	-75.380	Andesite unit	Andesite
11	2014 MI 14	4.972	-75.380	Volcanic mud flow	Volcanic mud flows deposits
12	2014 MI 15	4.971	-75.380	Volcanic mud flow	Volcanic mud flows deposits
13	2014 MI 16	4.963	-75.358	Andesite unit	Andesite
14	2014 MI 17	4.949	-75.478	Cajamarca Complex	Quartz phyllite
15	2014 MI 18	4.921	-75.446	Andesite unit	Andesite
16	2014 MI 19	4.919	-75.447	Andesite unit	Andesite
17	2014 MI 20	4.915	-75.446	Cajamarca Complex	Schist
18	2014 MI 21	4.915	-75.446	Cajamarca Complex	Schist

251 * WGS84 coordinate system

252

253 The thermal conductivity and the specific heat capacity (Table 2) associated to each lithology were
 254 calculated as the mean of the values obtained for all the samples belonging to the same unit, except
 255 for the thermal conductivity of the Andesite (NgQa). The thermal conductivity of sample 2014
 256 MI 16 was higher than the other samples taken at the same location and the mean would be
 257 significantly affected by this extreme value. Then, the median was used because it was considered
 258 to better represent the thermal conductivity of this lithologic unit. Sample 5 of the Quebradagrande
 259 Complex ($\lambda = 4.26 \text{ W m}^{-1} \text{ K}^{-1}$) was further excluded from the determination of the mean thermal
 260 conductivity because it was taken in a fault zone that did not represent the general characteristics of
 261 this geological complex.

262 The thermal conductivity values obtained for the Quebradagrande Complex and volcanic mudslides
 263 did not show significant variation since most of the values were close to $2.0 \text{ W m}^{-1} \text{ K}^{-1}$. The
 264 Andesite unit showed the lowest thermal conductivity value ($1.2 \text{ W m}^{-1} \text{ K}^{-1}$), while the Cajamarca
 265 Complex showed the highest value ($2.9 \text{ W m}^{-1} \text{ K}^{-1}$). Inferred heat capacity ranges from 815 to
 266 $1140 \text{ J Kg}^{-1} \text{ K}^{-1}$.

267 Table 2: Measured thermal conductivity λ and heat capacity C estimated from Waples and Waples
 268 (2004)

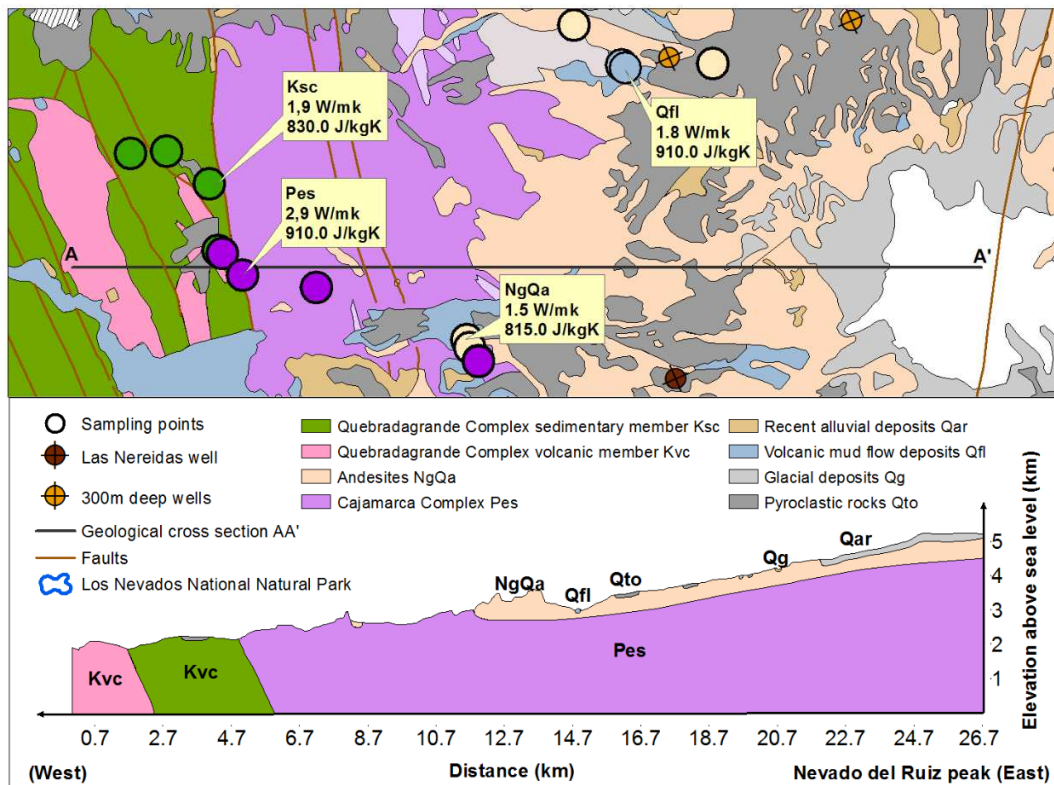
Lithologic unit	Sample code	Rock sample λ (W m ⁻¹ K ⁻¹)	Mean λ (W m ⁻¹ K ⁻¹)	Rock sample C (J kg ⁻¹ K ⁻¹)	Mean C (J kg ⁻¹ K ⁻¹)
Quebradagrande Complex sedimentary member (Ksc)	2014 MI 1	1.98	1.92	775	830
	2014 MI 2	1.15		775	
	2014 MI 3	2.63		910	
	2014 MI 5	4.26		860	
	2014 MI 8	1.34			
Andesite (NgQa)	2014 MI 12	1.33	1.23*	815	815
	2014 MI 13	0.91			
	2014 MI 16	3.29			
	2014 MI 18	1.12			
	2014 MI 19	1.08			
Volcanic mud flow deposits (Qfl)	2014 MI 14	1.59	1.89	840	840
	2014 MI 15	2.18			
Cajamarca Complex (Pes)	2014 MI 6	3.18	2.98	1090	910
	2014 MI 7	2.89		790	
	2014 MI 17	2.75		1090	
	2014 MI 20	2.87		790	
	2014 MI 21	3.22		790	

*Thermal conductivity of the andesite unit was calculated as the median of the sample values.

271 5.2 Geological cross-section

272 The thickness of the lithologic units in the geological cross-section AA' was based on a previous
 273 cross-section of the NDR volcano published by Central Hidroelectrica de Caldas (CHEC et al.,
 274 1983). Outcrops of the Quebradagrande and Cajamarca complexes are shown on this inferred
 275 geological cross-section (Figure 3). The Andesite unit is approximately 500 m thick (CHEC et al.,
 276 1983) and lies above the Cajamarca Complex. It is possible to see the different superficial deposits
 277 (Qto, Qar, Qg, Qfl) produced by the volcanic activity during the Quaternary period. The two
 278 members of the Quebradagrande Complex (Ksc y Kvc) are located on the west end of the cross-
 279 section and are dipping to the East.

280



281 Figure 3. Inferred geological cross-section AA' and thermal properties evaluated for lithological
 282 units Pes, NgQa, Qfl, Ksc. Geological map simplified from INGEOMINAS geological maps sheet
 283 Nos. 206 and 225 (Mosquera et al., 1998a; Mosquera et al., 1998b).
 284

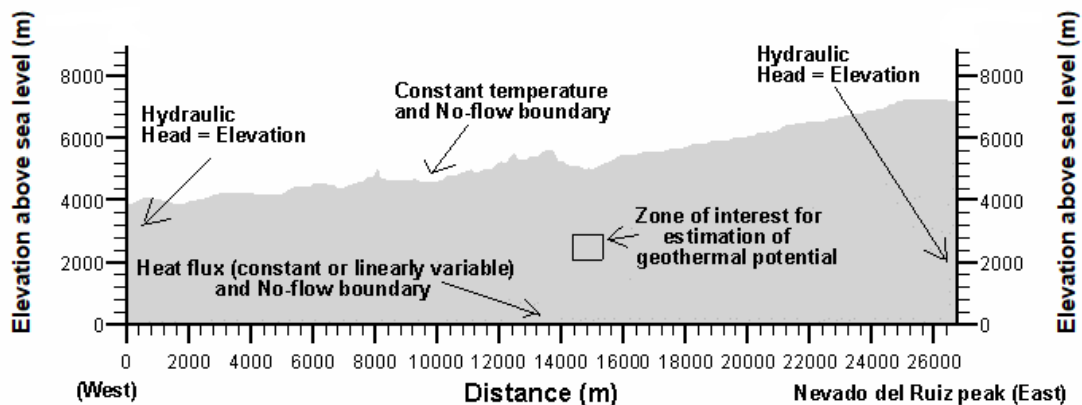
285

286 5.3 Underground temperature model

287 The simulated domain was based on the inferred geological cross-section AA' (Figure 3), where
 288 superficial geological deposits (Qar, Qfl, Qg, and Qto) were neglected, since their thickness was
 289 small enough to have a negligible influence on the underground temperature (Figure 4) due to their
 290 limited spatial extent. The zone of interest to quantify geothermal resources was delimited
 291 considering temperatures $> 150^{\circ}\text{C}$ and depth < 3 km, although groundwater flow and heat transfer
 292 was simulated over the whole cross section.

293 The triangular mesh built with GMSH has 4179 elements, which were refined close to the top of the
 294 domain to properly capture the topographic variations. Groundwater flow boundary conditions were

295 hydraulic heads equal to the topographic elevation at the lateral extremities of the model, while the
 296 top and bottom boundaries were considered impermeable (Figure 4). The top heat transfer boundary
 297 was a constant temperature determined from an elevation-dependent temperature profile, varying
 298 from +18 to -5 °C (CORPOCALDAS, 2007). Adiabatic conditions were set to the left and right of
 299 the domain. The bottom heat transfer boundary condition was a linearly variable heat flux defined
 300 considering the maximum, the minimum, and the mean heat flow values of the area. The minimum
 301 value, 0.12 W m^{-2} , was equal to the smallest heat flow in the study area, according to the Colombian
 302 heat flow map (INGEOMINAS, 2000); the mean value, 0.178 W m^{-2} , was evaluated from the
 303 geothermal gradient measured in the 300 m deep wells presented by Rojas (2012); the maximum
 304 value, 0.366 W m^{-2} , was estimated from the temperature gradient observed at the Nereidas well
 305 (Bernal et al., 2000).



306
 307 Figure 4. Model extension, boundary conditions, and selected zone of interest (1 km^2) for the
 308 estimation of the geothermal potential.

309
 310 An internal heat source was added to take into account the heat generation by the decay of
 311 radioactive elements. Concentrations of uranium, thorium and potassium for the average continental
 312 crust were considered (Turcotte and Schubert, 2014). The internal heat production was calculated
 313 as (Bucker and Rybach, 1996):

$$A = 10^{-5} \cdot \rho \cdot (9.52[U] + 2.56[Th] + 3.48[K]) \quad (6)$$

315 where A ($\mu\text{W m}^{-3}$) is the internal heat production, ρ (kg m^{-3}) is the average rock density, $[U]$ (ppm)
316 is the concentration of uranium, $[Th]$ (ppm) is the concentration of thorium, $[K]$ (%) is the
317 concentration of potassium. The value calculated for the average continental crust was $0.866 \mu\text{Wm}^{-3}$,
318 which was comprised within the range of common values for this parameter (Bédard et al., 2016).

319 A sensitivity analysis was conducted to define proper values for domain depth and mesh size. The
320 domain depth has an impact because the heat transfer under the simulated conditions is dominantly
321 vertical and affected by the irregular topography. For example, if the depth is lower, the heat source
322 is closer to the surface, affecting the simulated temperature and the final geothermal potential
323 estimation. The domain depth was defined on the right-hand side of the cross-section, where is
324 located the NDR peak (Figure 3). Depths of 3, 5, 7, 10, 12, 14, and 18 km were considered in the
325 sensitivity analysis. Mesh resolution was varied from 200 m to 600 m; since mesh is always
326 automatically refined close to the topography, these resolutions represent the average element size.
327 The criterion to choose the appropriate values was based on the variation of the simulated
328 temperature between two successive simulation results with varying depth or mesh resolution. The
329 final depth and mesh resolution were chosen when the minimum temperature variation was
330 observed between simulations. The selected model was 7 km deep and had an average mesh
331 element size of 400 m.

332 The thermal properties of the main geological units inferred from the field characterization and
333 hydraulic properties estimated according to Freeze and Cherry (1979) were used as inputs for the
334 numerical simulations (Table 4). Since samples were not available for the Kvc volcanic complex,
335 values equal to those of Ksc were assumed. The Kvc formation is, however, located on the left-hand
336 side of the geological cross-section and was believed to have a small effect on the simulated
337 temperature in the area of interest, which is located approximately 14 km away (Figure 4). This was
338 in fact verified by additional simulations whose results are not presented here.

339

340 Table 4. Properties of material used for numerical simulations

	Pes	NgQa	Kvc	Ksc
Saturated hydraulic conductivity K (m s^{-1})	1.0×10^{-11}	1×10^{-9}	1×10^{-10}	1×10^{-10}
Porosity n (-)	0.05	0.15	0.05	0.05
Thermal conductivity Case A ($\text{W m}^{-1} \text{K}^{-1}$)	2.98	1.22	1.92	1.92
Thermal conductivity Case B ($\text{W m}^{-1} \text{K}^{-1}$) (see Figure 5)	Layer 1:2.66 Layer 2:2.09 Layer 3:1.81	1.22	1.92	1.92
Specific heat capacity ($\text{J kg}^{-1} \text{K}^{-1}$)	910	815	830	830
Density (kg m^{-3})	2700	2650	2700	2700

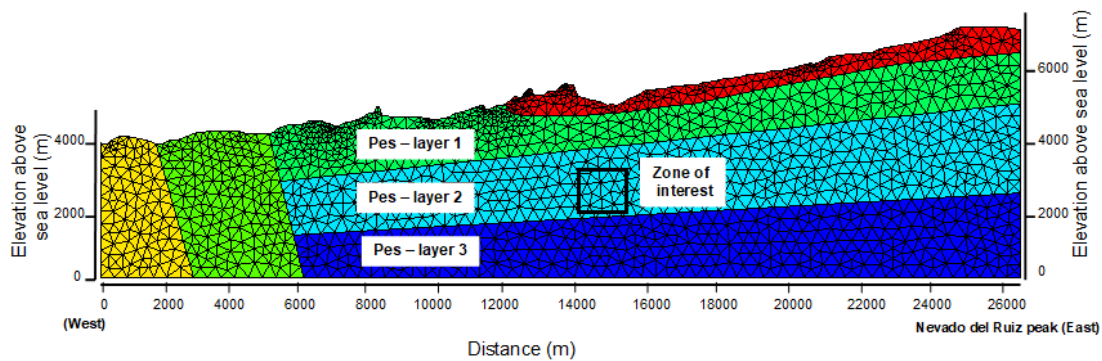
341

342 Two modeling scenarios were considered (Table 5) to compare a case characterized by constant
343 thermal conductivity in the Cajamarca Complex Pes (Case A), with another case characterized by a
344 temperature dependent thermal conductivity (Case B). Three sub-layers were defined in the
345 Cajamarca Complex for Case B (Figure 5), based on the temperature dependent thermal
346 conductivity calculated with the relation proposed by Clauser (2014):

$$347 \quad \lambda = A + \frac{B}{350 + T} \quad 0^\circ\text{C} \leq T \leq 800^\circ\text{C} \quad (7)$$

348 where A ($\text{W m}^{-1} \text{K}^{-1}$) = 0.75 and B (W m^{-1}) = 705 for metamorphic rocks.

349 Eq.(7) was applied to the simulated temperatures from Case A to define three regions with different
350 thermal conductivity in the metamorphic Cajamarca Complex, since a temperature dependent
351 thermal conductivity was not available in OpenGeoSys. This approach allowed investigating the
352 effect of temperature on thermal conductivity, although it is approximate.



353
 354 Figure 5. Triangular mesh and sub-layers 1, 2, and 3 in the Cajamarca metamorphic complex (Pes)
 355 close to the zone of interest, for simulation scenario Case B.

356

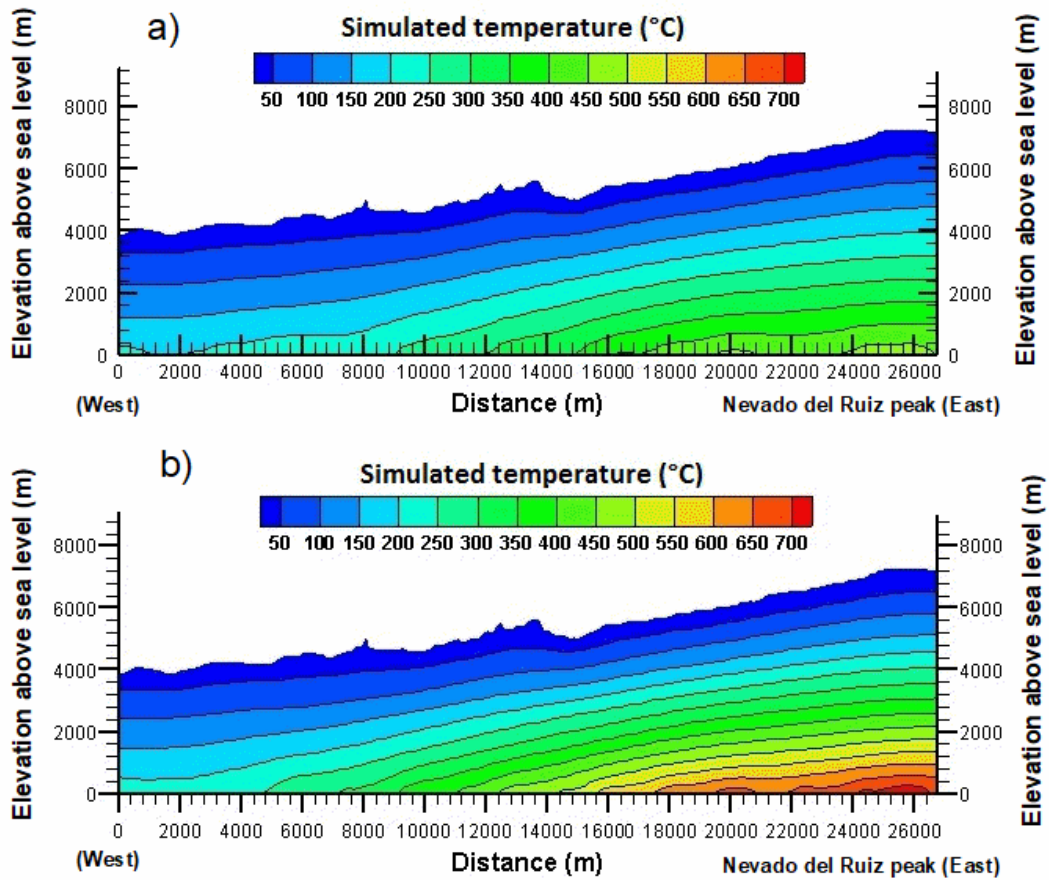
357 Table 5. Modeling scenarios considered

Scenario	Description
Case A	Constant thermal conductivity for the Cajamarca Complex (Pes)
Case B	Temperature dependent thermal conductivity for the Cajamarca Complex (Pes)

358

359

360 The maximum temperature simulated for Case A was 532 °C at the bottom right-hand side of the
 361 profile, where the largest heat flux (0.366 W m^{-2}) was applied as a bottom boundary condition
 362 (Figure 6a). The temperature was greater than 150°C in the area of interest at a distance of 14–15
 363 km and at a depth of 2-3 km, indicating that high-enthalpy geothermal resources (Lee, 1996) are
 364 located outside of the Los Nevados NNP, where they may be exploited.



365

366

Figure 6. Simulated temperature distribution for a) Case A and b) Case B.

367

The maximum simulated temperature increased in Case B (Figure 6b), with a temperature dependent thermal conductivity in the Cajamarca Complex (Pes). This temperature increase was due to the lower thermal conductivity providing insulation in the deeper region of the cross-section.

368

369

The maximum simulated temperature was now 753°C, while it was 532°C in Case A. Nevertheless,

370

the increase in temperature was somewhat more moderate in the area of interest, with an average

371

increase of 45°C. Simulated temperatures were now greater than 200°C in almost all the area of

372

interest. This scenario was considered as more realistic, since it takes into account the decreasing of

373

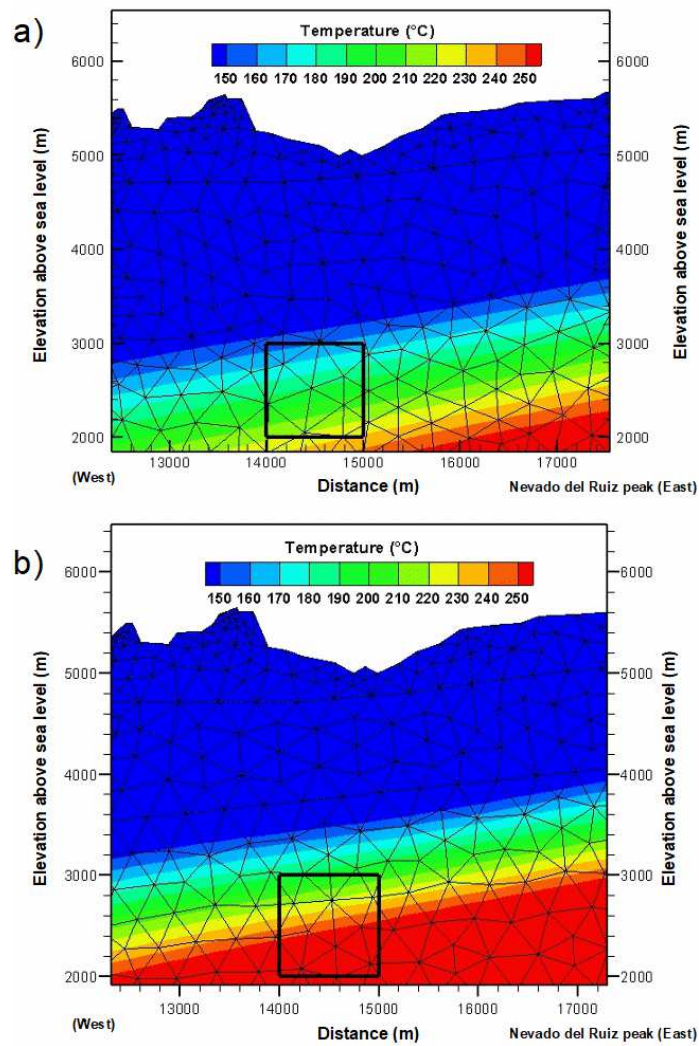
thermal conductivity with temperature, although still approximate.

375 The influence of the internal heat production due to the radioactive decay appeared not be
376 significant since a small value of internal heat generation was calculated ($0.866 \mu\text{W m}^{-3}$), compared
377 to the heat flux applied to the bottom boundary (mean value of 0.2 W m^{-3}).

378

379 **5.4 Geothermal resource evaluation**

380 In order to quantify the influence of the temperature at depth T_d and the recovery factor R on the
381 geothermal resources evaluation, Case A and Case B were considered. The simulated temperatures
382 in the area of interest for simulation scenarios Case A and Case B are shown in Figure 7, where the
383 triangular mesh is also illustrated. Using Eq.(4), the available subsurface heat Q_R was estimated,
384 exporting the simulated temperature at points uniformly distributed over the area of interest along
385 five 1000 m high vertical segments (from a depth of 2000 m to 3000 m) located 200 m apart. Since
386 each segment had 10 points along its height, the area A associated with each point is $22,000 \text{ m}^2$
387 ($200 \text{ m} \times 110 \text{ m}$): the density and heat capacity of the Cajamarca Complex (Table 4) were
388 considered to calculate with Eq.(5) the geothermal potential P_G for a 30 y exploitation period with
389 $R=2.4\%$ as recovery factor (Table 6). The geothermal potential was larger for Case B, since higher
390 temperatures were obtained using a temperature dependent thermal conductivity, for the same heat
391 flux bottom boundary condition. Nevertheless, both geothermal power resources were on the same
392 order of magnitude (1.36×10^{-2} and $1.67 \times 10^{-2} \text{ MW}_t \text{ m}^{-1}$).



393

394 Figure 7. Simulated temperatures and triangular mesh in the zone of interest for a) Case A and b)

395

for Case B

396

397

Table 6. Geothermal resource evaluation per km² of potential reservoir section

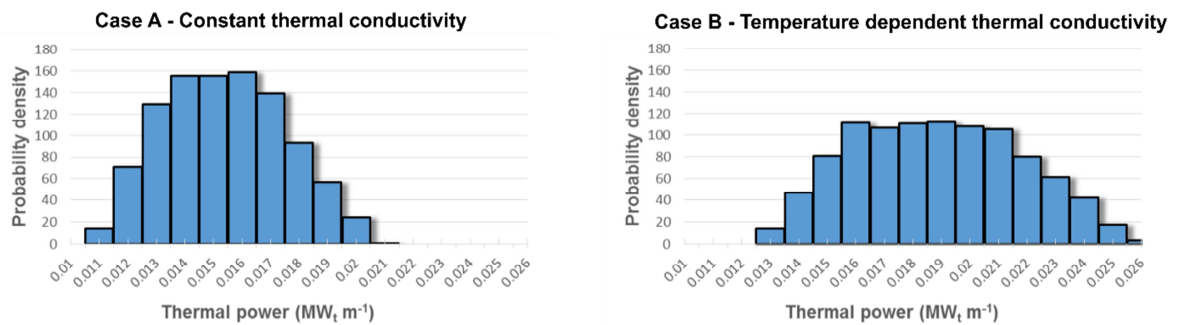
Scenario	Q_R Total energy ($J m^{-1}$) (Eq.4)	P_G Geothermal power ($MW_t m^{-1}$) (Eq.5)
Case A	5.38×10^{14}	1.36×10^{-2}
Case B	6.60×10^{14}	1.67×10^{-2}

398

399 5.5 Uncertainty analysis

400 Uncertainty analysis of the geothermal potential was conducted for the area of interest (Figure 4),
401 using the temperature variation ΔT and the recovery factor R as input variables with 10000 Monte
402 Carlo iterations. Uniform distributions were used to define the variation of the parameters.
403 Recovery factor varied from 2.4% to 3% and the temperature variation from 160.5 °C to 235°C.
404 The temperature intervals between 156 °C and 239 °C and between 183°C and 301°C were obtained
405 for the two scenarios, Case A and Case B, respectively. The mean thermal energy for Case A,
406 considering homogenous thermal conductivity in the Cajamarca Complex, was $1.54 \times 10^{-2} \text{ MW}_t \text{ m}^{-1}$
407 with a standard deviation of $2.1 \times 10^{-3} \text{ MW}_t \text{ m}^{-1}$ (Figure 8). The minimum and maximum values
408 were $1.08 \times 10^{-2} \text{ MW}_t \text{ m}^{-1}$ and $2.06 \times 10^{-2} \text{ MW}_t \text{ m}^{-1}$, respectively. For an approximate reservoir
409 width of 5 km, the mean estimated geothermal potential was 77 MW_t , while the minimum and
410 maximum values were 54 MW_t and 103 MW_t . This reservoir width corresponds to the average
411 outcrop width of the Cajamarca Complex, as it can be observed in the geological map (Figure 2).
412 The mean thermal energy for Case B, considering temperature dependent thermal conductivity in
413 the Cajamarca Complex, was $1.88 \times 10^{-2} \text{ MW}_t \text{ m}^{-1}$ with a standard deviation of $2.91 \times 10^{-3} \text{ MW}_t \text{ m}^{-1}$
414 ¹. The minimum and maximum values were $1.28 \times 10^{-2} \text{ MW}_t \text{ m}^{-1}$ and $2.59 \times 10^{-2} \text{ MW}_t \text{ m}^{-1}$,
415 respectively (Figure 8). Considering the same reservoir width of 5 km, the mean estimated
416 geothermal potential was now 94 MW_t , while the minimum and maximum values were 64 MW_t and
417 130 MW_t , respectively.

418



419

420

Figure 8. Geothermal power uncertainty analysis conducted with RISK.

421

422 6 Discussion

423 This paper presented an estimation of the geothermal potential of an area of approximately 1 km² to
 424 the northwest of the Nevado Del Ruiz (NDR) volcano (Colombia). The work consisted in collecting
 425 rock samples in surface outcrops, measuring thermal conductivity of the rock samples with a needle
 426 probe in the laboratory, estimating heat capacity based on mesoscopic description of rock type,
 427 inferring a geological cross-section, simulating temperature at depth with numerical modeling of
 428 steady-state groundwater flow and heat transfer and conducting an uncertainty analysis using
 429 Monte Carlo simulations.

430 Numerical modeling based on the finite element method is recommended for the estimation of
 431 geothermal potential (Aravena et al., 2016), since it provides a rigorous way to evaluate and
 432 understand conceptual models and the system heat transfer mechanisms. Similarly, González-
 433 Garcia and Jessell (2016) stated that numerical modeling of heat and mass transfer in a
 434 hydrothermal system is a proper tool to provide a quantitative estimate of geothermal resources, as
 435 well as to aid in the sustainable management of these resources. Therefore, numerical modeling was
 436 used here as a tool helping to deal with topography and thermal conductivity distribution
 437 constrained by the inferred geology, to provide an estimation of the geothermal resources in the
 438 study area. Modeling results indicated that the Cajamarca Complex, characterized by a thermal

439 conductivity of $2.9 \text{ W m}^{-1} \text{ K}^{-1}$ can host potential basement reservoirs, as also suggested by
440 Almaguer (2013), where the presence of secondary porosity will allow water circulation since the
441 rock matrix has a low primary porosity. The Andesite unit, characterized by low thermal
442 conductivity of $1.2 \text{ W m}^{-1} \text{ K}^{-1}$, can provide insulation or thermal blanketing effect.

443 The average thermal power estimated with Monte Carlo simulations was $1.54 \times 10^{-2} \text{ MW}_t \text{ m}^{-1}$
444 (homogenous thermal conductivity) and $1.88 \times 10^{-2} \text{ MW}_t \text{ m}^{-1}$ (temperature dependent thermal
445 conductivity) per meter of thickness of the potential reservoir and for an area of 1 km^2 located
446 outside the Los Nevados NNP. This estimation is based on thermal conductivity measurements in
447 surface samples and on the simulation of the geothermal gradient with a numerical model to
448 anticipate temperature up to a depth of 2 km. The use of these variables and the hypothesis selected
449 to estimate the temperature at depth can obviously affect the resources evaluation. However there is
450 currently a lack of information about the behavior of the rock thermal conductivity at depth that
451 could be obtained in the future from deep wells to further constrain temperature observations and
452 calibrate the numerical model. Nevertheless, with available information in the study area facing
453 early exploration stage, the estimated geothermal resource is thought to be representative of the
454 current state of knowledge that will be improved as exploration proceeds to verify additional
455 hypothesis that can influence heat transfer mechanisms at depth.

456 A utilization efficiency factor was used to evaluate the electrical generation potential. This factor
457 depends on the geothermal fluid temperature (Williams et al., 2008) and is calculated by comparing
458 the actual power output to the maximum theoretical power that could be produced from the given
459 geothermal fluid (DiPippo, 2012). An efficiency of 0.4 has been reported for systems of high
460 temperature (above $150 \text{ }^\circ\text{C}$; Muffler and Cataldi, 1978; Williams et al., 2008).

461 Further research steps shall consider the heterogeneity of the lithologic units, in other to identify
462 and collect samples of the different type of rocks constituting the formations and estimate its
463 thermal conductivity distribution. This additional work is important for the highly heterogeneous
464 formations like the Quebradagrande and the Cajamarca complexes. Additional thermal conductivity

465 measurements will further help to take into account the impact of heterogeneity in the Monte Carlo
466 simulations and quantify its effect for the resource estimation. Only temperature at depth and
467 recovery factor were included in this work for the uncertainty analysis. Petrophysical properties
468 could be taken into account to help scale up thermal properties and better define their distribution in
469 next research steps, when further deep well data becomes available, to finally refine Monte Carlo
470 analysis of geothermal resources.

471

472 **7 Conclusions**

473 The thermal power estimated in this study can be compared to the electric power of 50 MW_e
474 mentioned by Mejía et al. (2014), assuming a utilization factor of 0.4 and a reservoir width of 5 km.
475 The electric power would consequently be comprised within the range 30–40 MW_e for the potential
476 reservoir considering both scenarios (Case A and B), thus close to the estimation mentioned by
477 Mejía et al. (2014). Nevertheless, the current study provides a more detailed analysis of the NDR
478 geothermal resource potential by describing the complete methodology to obtain the final power
479 estimates.

480 The uncertainty analysis allowed identifying the influence of the reservoir temperature and the
481 recovery factor as input variables on the geothermal power estimate. A change in the reservoir
482 temperature has a greater effect on the estimated thermal power than a change in the possible
483 recovery factor.

484 An accurate measurement of the heat flow over the study area, with continuous downhole
485 temperature profiles and thermal conductivity measurements on core samples, will help to better
486 estimate and model the temperature at depth to reduce resource uncertainty in the future. 3D
487 geomodeling combined with new deep exploratory wells will further improve the inferred
488 geological cross-section to the benefit of the geothermal potential estimation. Geomodeling will be
489 particularly useful to better characterize the geological contact between the Cajamarca Complex,
490 potential fractured reservoirs and the Andesite unit since this contact is a key factor to evaluate the

491 temperature at depth. Additionally, since the Cajamarca Complex is highly heterogeneous, detailed
492 field investigations are required to improve its description. Further work will focus on the
493 characterization of fault systems associated with hot springs and on the numerical simulation of
494 reservoir exploitation with production and injection wells. Such logical steps are needed to move
495 forward with the development of geothermal energy in Colombia, providing critical knowledge to
496 support energy decisions.

497 This work is a valuable contribution to geothermal resource assessment that can be applied to
498 eventually evaluate the total resource in Colombia. Geothermal resources still has to be defined at
499 the Tufiño-Chiles-Cerro Negro geothermal system at the Colombia-Ecuador border, the Azufral,
500 Purace, and Galeras volcanoes, and the Paipa and San Diego areas, which are the regions where
501 exploration studies have been conducted or hydrothermal systems have been observed (Alfaro,
502 2015). The same methodology can be useful for other countries of South America. Several countries
503 such as Bolivia, Argentina, Ecuador and Peru are looking for geothermal resources exploitation
504 although no geothermal capacity was installed in this region up to 2015 (Bertani, 2016). The first
505 geothermal power plant in South America started delivering electricity to the interconnected grid
506 deserving northern Chile in March 2017², highlighting an important step in the history of
507 geothermal energy in South America. Geothermal resource assessment studies are required to
508 support the development of such projects.

509

510 **8 Acknowledgments**

511 This work was conducted in the context of a research project funded by the Universidad de
512 Medellín (Medellín, Colombia) in collaboration with the Institut national de la recherche
513 scientifique (Québec, Canada). Thanks to the Canadian Department of Foreign Affairs, Trade and
514 Development who assigned the Emerging Leaders in the Americas Program scholarships to Maria

² <http://www.cega.ing.uchile.cl/en/noticias/primer-planta-geotermica-de-sudamerica-comienza-sus-operaciones-en-el-norte-de-chile/>

515 Isabel Vélez and Sebastian Cordoba in 2015. Thanks to Thomas Kalbacher for his help with the
516 software OpenGeoSys and to two anonymous reviewers contributing to the improvement of the
517 original paper.

518 The IGCP, UNESCO, and IUGS are finally acknowledged since this work is part of the project
519 “IGCP 636-Unifying international research forces to unlock and strengthen geothermal exploitation
520 of the Americas and Europe”, currently funded by UNESCO (United Nations Educational,
521 Scientific and Cultural Organization) and IUGS (International Union of Geological Sciences)
522 within the International Geoscience Programme (IGCP).

523

524 **References**

525 Alfaro, C. 2015. Improvement of perception of the geothermal energy as a potential source of
526 electrical energy in Colombia, country update. Paper presented at the World Geothermal Congress,
527 Melbourne, Australia. 15 pp.

528 Almaguer, J.L. 2013. Estudios magnetotélúrico con fines de interés geotérmico en sector Norte del
529 Nevado del Ruíz, Colombia. MSc thesis, Universidad Nacional Autónoma de México. 139 pp.

530 ASTM - American Society for Testing and Materials. 2008. Standard test method for determination
531 of thermal conductivity of soil and soft rock by thermal needle probe procedure (Vol. D5334 - 08),
532 9 pp.

533 Arango, E.E., Buitrago, A.J., Cataldi, R., Ferrara, G.C., Panichi, C., Villegas, V.J. 1970.
534 Preliminary study on the Ruiz geothermal project (Colombia). *Geothermics*, 2, Part 1: 43-56. doi:
535 10.1016/0375-6505(70)90005-2.

536 Aravena, D., Muñoz, M., Morata, D., Lahsen, A., Parada, M. Á., Dobson, P. 2016. Assessment of
537 high enthalpy geothermal resources and promising areas of Chile. *Geothermics*, 59, Part A: 1-13.
538 doi: 10.1016/j.geothermics.2015.09.001.

539 Barylo, A. 2000. Assesment of the energy potential of the Beregovsky geothermal system, Ukraine
540 Geothermal Training Programme. Iceland: 29-42.

541 Bédard, K., Comeau, F.-A. Millet, E., Raymond, J., Malo, M., Gloaguen, E. 2016. Évaluation des
542 ressources géothermiques du bassin des Basses-Terres du Saint-Laurent. Research Report 1659.
543 Institut national de la recherche scientifique - Centre Eau Terre Environnement. 100 pp.

544 Bernal N.F., Ramirez G., Alfaro C.V. 2000. Mapa geotérmico de Colombia. Versión 1.0. Escala
545 1:1'500.000. Memoria explicativa. Exploración y Evaluación de Recursos Geotérmicos. Instituto de
546 investigación e información geocientífica, minero-ambiental y nuclea INGEOMINAS. 51 pp.

- 547 Bertani, R. 2009. Geothermal energy: an overview on resources and potential. Proceedings of the
548 International Conference on National Development of Geothermal Energy Use and International
549 Course/EGEC Business Seminar on organization of successful development of a geothermal
550 project, k. Popovski, A.Vranovska, S. Popovska Vasilevska, Editors. 19 pp.
- 551 Bertani, R. 2016. Geothermal power generation in the world 2010-2014 update report. *Geothermics*,
552 60: 31-43. doi:<http://dx.doi.org/10.1016/j.geothermics.2015.11.003>.
- 553 Böttcher, N., Watanabe, N., Görke, U.-J., Kolditz, O. 2016. Geoenergy Modeling I. Geothermal
554 Processes in Fractured Porous Media. SpringerBriefs in Energy. Computational Modeling of
555 Energy Systems. 117 pp.
- 556 Bucker, C., Rybach, L. 1996. A simple method to determine heat production from gamma-ray logs.
557 *Marine and Petroleum Geology*, 13(4): 373–375.
- 558 Calcagno, P., Baujard, C., Guillou-Frottier, L., Dagallier, A., Genter, A. 2014. Estimation of the
559 deep geothermal potential within the Tertiary Limagne basin (French Massif Central): An integrated
560 3D geological and thermal approach. *Geothermics*, 51(0): 496-508. doi:
561 <http://dx.doi.org/10.1016/j.geothermics.2014.02.002>.
- 562 Carslaw, H. S., & Jaeger, J. C. (1947). *Conduction of Heat in Solids*. Oxford,UK: Oxford
563 University Press.
- 564 CHEC - Central Hidroeléctrica de Caldas, Instituto Colombiano de Energía Eléctrica, Consultoría
565 Técnica Colombiana Ltda, Geotérmica Italiana. 1983. Investigación Geotérmica Macizo Volcánico
566 del Ruíz. Fase II, Etapa A (Vol. II, III). Bogotá.
- 567 Clauser, C. 2014. Thermal Storage and Transport Properties of Rocks, II: Thermal Conductivity and
568 Diffusivity. *Encyclopedia of Solid Earth Geophysics*. Part of the series *Encyclopedia of Earth
569 Sciences Series*. Springer Netherlands. Editors: Harsh K. Gupta. pp. 1431-1448.
- 570 CORPOCALDAS 2007. Plan de manejo de los páramos del departamento de Caldas. Technical
571 report. 133 pp.
- 572 Decagon Devices Inc. 2008. KD2 Pro Thermal properties analyzer operator's manual version 12.
573 Decagon Devices, Inc. 72 pp.
- 574 DiPippo, R. 2012. Geothermal power plants: principles, applications, case studies and
575 environmental impact (3 ed.). Massachusetts, UE: Butterworth-Heinemann. 624 pp.
- 576 Forero, J.A. 2012. Caracterización de las alteraciones hidrotermales en el flanco Noroccidental del
577 Volcán Nevado del Ruiz, Colombia. MSc thesis, Universidad Nacional de Colombia, Bogotá. 121
578 pp.
- 579 Freeze, A.R., Cherry, J.A. 1979. *Groundwater*. Prentice-Hall. 604 pp.
- 580 Fridleifsson, I. B. 2003. Status of geothermal energy amongst the world's energy sources.
581 *Geothermics*, 32(4–6): 379–388. doi:<http://dx.doi.org/10.1016/j.geothermics.2003.07.004>.

- 582 Geuzaine, C., Remacle, J-F. 2009. A three-dimensional finite element mesh generator with built-in
583 pre- and post-processing facilities. *International Journal for Numerical Methods in*
584 *Engineering* 79(11): 1309-1331.
- 585 González-García, J., Jessell M. 2016. A 3D geological model for the Ruiz-Tolima Volcanic Massif
586 (Colombia): Assessment of geological uncertainty using a stochastic approach based on Bézier
587 curve design. *Tectonophysics* 687 (26): 139–157.
- 588 González-García J., Hauser J., Annetts D., Franco J., Vallejo E., Regenauer-Lieb K. 2015.
589 Nevado Del Ruiz Volcano (Colombia): A 3D Model Combining Geological and
590 Geophysical Information. *Proceedings World Geothermal Congress, Melbourne, Australia.*
591
- 592 González, H. 2001. Geología de las planchas 206 Manizales y 225 Nevado del Ruíz. Memoria
593 explicativa. Instituto de investigación e información geocientífica, minero-ambiental y nuclear,
594 INGEOMINAS, Bogotá. 93 pp.
- 595 INGEOMINAS 2000. Mapa de flujos de calor-
- 596 Invernizzi, C., Pierantoni P.P., Chiodi A., Maffucci R., Corrado S., Baez W., Tassi F., Giordano G.,
597 Viramonte J., 2014. Preliminary assessment of the geothermal potential of Rosario de la Frontera
598 area (Salta, NW Argentina): Insight from hydro-geological, hydro-geochemical and structural
599 investigations. *Journal of South American Earth Sciences* 54: 20–36.
- 600 Lee, K.C. 1996. Classification of geothermal resources – an engineering approach. *Proceedings,*
601 *Twenty-First Workshop on Geothermal Reservoir Engineering, Stanford University, Stanford,*
602 *California, January 22–24. SGP-TR-151, 8 pp.*
- 603 Londoño, J. M., Sudo, Y. 2002. Velocity structure and a seismic model for Nevado del Ruiz
604 Volcano (Colombia). *Journal of Volcanology and Geothermal Research*, 119 (1-4): 61-87. doi:
605 [http://dx.doi.org/10.1016/S0377-0273\(02\)00306-2](http://dx.doi.org/10.1016/S0377-0273(02)00306-2).
- 606 Mejía, E., Rayo, L., Méndez, J., Echeverri, J. 2014. Geothermal development in Colombia. Short
607 Course VI on Utilization of Low- and Medium-Enthalpy Geothermal Resources and Financial
608 Aspects of Utilization, Santa Tecla, El Salvador. 7 pp.
- 609 Mejía, E., Velandia, F., Zuluaga, C.A., López, J.A., Cramer, T. 2012. Análisis estructural al noreste
610 del Volcán Nevado de Ruíz Colombia – Aporte a la Exploración Geotérmica. *Boletín de Geología,*
611 *34(1): 27-41.*
- 612 Melson, W.G., Allan, J.F., Jerez, D.R., Nelen, J., Calvache, M.L., Williams, S.N., Fournelle J.,
613 Perfit, M. 1990. Water contents, temperatures and diversity of the magmas of the catastrophic
614 eruption of Nevado del Ruiz, Colombia, November 13, 1985. *Journal of Volcanology and*
615 *Geothermal Research*, 41 (1): 97-126. doi:[http://dx.doi.org/10.1016/0377-0273\(90\)90085-T](http://dx.doi.org/10.1016/0377-0273(90)90085-T).
- 616 Monsalve, M.L., Rodríguez, G.I., Méndez, R.A., Bernal, N.F. 1998. Geology of the Well Nereidas
617 1, Nevado Del Ruiz Volcano, Colombia *Geothermal Resources Council* 22, 6 pp.

- 618 Mosquera, D., Marín, P., Vesga, C., González, H. 1998a. Geología de la Plancha 225 Nevado del
619 Ruíz.
- 620 Mosquera, D., Marín, P., Vesga, C., González, H., Maya, M. 1998b. Geología de la Plancha 206
621 Manizales.
- 622 Muffler, P., Cataldi, R. 1978. Methods for regional assessment of geothermal resources.
623 *Geothermics*, 7 (2), 53–89. doi: 10.1016/0375-6505 (78)90002-0
- 624 Naranjo, J.L., Sigurdsson, H., Carey, S.N., Fritz, W. 1986. Eruption of the Nevado del Ruiz
625 Volcano, Colombia, On 13 November 1985: Tephra Fall and Lahars. *Science*, 233 (4767): 961–963.
626 doi:10.1126/science.233.4767.961
- 627 Ofwona, C. 2008. Geothermal resource assessment-Case example, Olkaria I. Geothermal Training
628 Programme, 8 pp.
- 629 Parques Nacionales Naturales de Colombia - Dirección Territorial Noroccidente. 2007. Plan de
630 Manejo 2007-2011. Parque Nacional Natural de Los Nevados. 37 pp.
- 631 Rayo-Rocha, L., Zuluaga, C.A. 2011. Procesos Magmáticos En El Volcán Nevado Del Ruiz: Un
632 Análisis Cuantitativo Textural. *Boletín de Geología*, 33(2): 59-72.
- 633 Rojas, O.E. 2012. Contribución al modelo geotérmico asociado al sistema volcánico Nevado del
634 Ruiz-Colombia, por medio del análisis de la relación entre la susceptibilidad magnética,
635 conductividad eléctrica y térmica del sistema. MSc thesis, Universidad Nacional de Colombia,
636 Bogotá. 183 pp.
- 637 Stefánsson, V. 1998. Estimate of the world geothermal potential. Geothermal training programme,
638 Iceland. 10 pp. The United Nations University. 20th Anniversary Workshop.
- 639 Stefánsson, V. 2005. World Geothermal Assessment. Proceedings World Geothermal Congress.
640 Amtalya, Turkey. 6 pp.
- 641 Stix, J., Layne, G.D., Williams S.N. 2003. Mechanisms of degassing at Nevado del Ruiz volcano,
642 Colombia. *Journal of the Geological Society, London*, 160: 507-521.
- 643 Thouret, J.-C. 1990. Effects of the November 13, 1985 eruption on the snow pack and ice cap of
644 Nevado del Ruiz volcano, Colombia. *Journal of Volcanology and Geothermal Research*, 41 (1):
645 177-201. doi:http://dx.doi.org/10.1016/0377-0273 (90)90088-W.
- 646 Trenkamp, R., Kellogg, J.N., Freymueller, J.T., Mora, H.P. 2002. Wide plate margin deformation,
647 southern Central America and northwestern South America, CASA GPS observations. *Journal of*
648 *South American Earth Sciences*, 15 (2): 157–171. doi:http://dx.doi.org/10.1016/S0895-9811
649 (02)00018-4.
- 650 Turcotte, D.L., Schubert, G. 2014. *Geodynamics*. Cambridge University Press. 657 pp.
- 651 Vatin-Pérignon, N., Goemans, P., Oliver, R.A., Parra, E. 1990. Evaluation of magmatic processes
652 for the products of the Nevado del Ruiz Volcano, Colombia from geochemical and petrological

- 653 data. *Journal of Volcanology and Geothermal Research*, 41 (1-4): 153-176. doi: 10.1016/0377-0273
654 (90)90087-v.
- 655 Walsh, W. 2013. Geothermal resource assessment of the Clarke Lake Gas Field, Fort Nelson,
656 British Columbia. *Bulletin of Canadian Petroleum Geology*, 61 (3): 241-251.
- 657 Waples, D., Waples, J. 2004. A Review and Evaluation of Specific Heat Capacities of Rocks,
658 Minerals, and Subsurface Fluids. Part 1: Minerals and Nonporous Rocks. *Natural Resources*
659 *Research*, 13 (2), 97–122. doi: 10.1023/B:NARR.0000032647.41046.e7.
- 660 Westaway, R., Younger, P.L., 2013. Accounting for palaeoclimate and topography: A rigorous
661 approach to correction of the British geothermal dataset. *Geothermics* 48: 31-51.
- 662 Williams, C. F., Reed, M. J., Mariner, R. H. 2008. A review of methods applied by the US
663 Geological Survey in the assessment of identified geothermal resources. US Geological Survey
664 Open-File Report, 1296, 27. 30 pp.
- 665 Yang, F., Liu, S., Liu, J., Pang, Z., Zhou, D. 2015. Combined Monte Carlo Simulation and
666 Geological Modeling for Geothermal Resource Assessment: a Case Study of the Xiongqian
667 Geothermal Field, China. *World Geothermal Congress, Melbourne, Australia*. 8 pp.

Highlights

- A methodology to quantify geothermal potential is proposed.
- Laboratory thermal conductivity measurements on rock samples.
- Coupled groundwater flow and heat transfer modeling in geological porous media.